

Numerical simulation of NQR/NMR: Applications in quantum computing

Denimar Possa, Anderson C. Gaudio, Jair C.C. Freitas*

Departamento de Física, Universidade Federal do Espírito Santo, 29075-910 Vitória, ES, Brazil

ARTICLE INFO

Article history:

Received 23 December 2010

Revised 18 January 2011

Available online 26 January 2011

Keywords:

NQR

NMR

Quantum computing

Numerical simulation

Density matrix

Average Hamiltonian

ABSTRACT

A numerical simulation program able to simulate nuclear quadrupole resonance (NQR) as well as nuclear magnetic resonance (NMR) experiments is presented, written using the Mathematica package, aiming especially applications in quantum computing. The program makes use of the interaction picture to compute the effect of the relevant nuclear spin interactions, without any assumption about the relative size of each interaction. This makes the program flexible and versatile, being useful in a wide range of experimental situations, going from NQR (at zero or under small applied magnetic field) to high-field NMR experiments. Some conditions specifically required for quantum computing applications are implemented in the program, such as the possibility of use of elliptically polarized radiofrequency and the inclusion of first- and second-order terms in the average Hamiltonian expansion. A number of examples dealing with simple NQR and quadrupole-perturbed NMR experiments are presented, along with the proposal of experiments to create quantum pseudopure states and logic gates using NQR. The program and the various application examples are freely available through the link http://www.profanderson.net/files/nmr_nqr.php.

© 2011 Elsevier Inc. All rights reserved.

1. Introduction

Computer programs for numerical simulation are an important tool for analysis and design of nuclear magnetic resonance (NMR) experiments and are widely used by the scientific community, especially regarding solid-state NMR [1–7]. Most of these programs are based on the calculation of the temporal evolution of the density operator corresponding to the spin system after a sequence of radiofrequency (RF) pulses. The main mathematical difficulty of this problem stems from the explicit time dependence of the RF Hamiltonian; in general this difficulty is removed by describing the dynamical evolution of the system as viewed from the so-called rotating reference frame [8,9]. In its conventional form, this approach is limited to systems presenting a symmetry compatible with the rotating reference frame, e.g., for nuclear spins subjected to an intense and static magnetic field, where the Zeeman interaction is dominant and the other interactions are treated as small perturbations. In other cases, where this symmetry is not present, a more general description of time-dependent interactions is required, involving the use of interaction frames (of which the rotating frame is a particular case) [10]. In the appropriate interaction frame, the quantum states evolve in time only due to the RF Hamiltonian, whatever the form of the static Hamiltonian (before the application of the RF pulses). Under certain conditions, the RF Hamiltonian is nearly stationary in the interaction frame and the

problem of temporal evolution of states can be solved by using average Hamiltonian theory [11,12]. This flexibility in the description of the system dynamics enables the development of simulation programs of broad applicability, which can be used for high-field NMR spectroscopy as well as for other magnetic resonance techniques, where the Zeeman interaction is not the dominant one, as it is the case of nuclear quadrupole resonance (NQR) [13–16].

This paper presents a program for the numerical simulation of NQR and NMR experiments developed using the Mathematica software [17]. The program is of high flexibility, allowing the simulation of experiments for nuclei with arbitrary spin, taking into account the combination of quadrupole and Zeeman interactions with no restriction on the relative size of each coupling and for any orientation of the corresponding principal axes. Moreover, it can be easily generalized and expanded to include other interactions. Another important feature of the program is the possibility to include RF pulses linearly polarized in any direction, as well as combinations of them, allowing then the simulation of experiments involving multifrequency pulses and elliptically polarized pulses. The orientation of the detecting coil is also arbitrary, allowing the use of different directions for excitation and phase-sensitive detection. As the spin dynamics is calculated by means of average Hamiltonian theory, higher-order effects can be easily addressed, which makes possible the simulation of experiments involving two-photon transitions in NQR [18,19].

These features are especially important for the design of experiments aiming the use of NQR as a tool to implement ensemble

* Corresponding author.

E-mail address: jairccfreitas@yahoo.com.br (J.C.C. Freitas).

quantum computing. It is well known that high-field NMR, both for liquids and liquid crystals, provides an efficient way to implement ensemble quantum computing operations [20–37]. Both NMR and NQR have drawbacks related to the intrinsic limitations of using pseudopure states in ensembles, as opposed to “true” quantum computing systems involving pure quantum states, and to the scalability to large numbers of q-bits. Most reports of quantum computing by bulk NMR to date involve small number of q-bits: up to ca. 10 for coupled spin 1/2 systems and up to 3 for quadrupolar nuclei [37]. Nonetheless, bulk NMR remains the simplest experimental technique used for demonstration of quantum computing principles and for simulation of quantum problems in systems with small number of q-bits (typically 2–5) [20,21,23,31,33,34,37]. Given the similarity to NMR, one can foresee the same scenario regarding the use of NQR for quantum computing, where the number of q-bits is limited to 3 (at least for pure NQR). However, as with NMR, NQR can be quite useful as an experimentally simple method for demonstrating quantum information processing and for performing quantum simulations. The main potential advantage of NQR (either under zero or small external magnetic field) as compared to high-field NMR is the much reduced cost of the spectrometers used for NQR experiments (which do not need superconducting magnets). Thus, it is worth investigating about the possibilities of use of NQR for quantum computing, which requires the development of methods for simulation of NQR dynamics. Furman et al. [38] proposed a method for obtaining pseudopure quantum states for two q-bits using NQR without any static magnetic field, but employing two RF fields with different phases, amplitudes and directions. This method is not easy to implement and, to the best of our knowledge, no experimental realization of it has ever appeared. In this work, we propose a different approach to the use of NQR for quantum computing, involving the use of circularly polarized RF fields and double-quantum excitation for the creation of pseudopure states and of simple logical gates. As these methods have already been implemented experimentally in a different NQR context [18,19,39,40], the extension of their use to encompass experiments related to quantum computing is apparently straightforward. Thus, some of the various simulation examples presented in this work describe concrete proposals to perform quantum computing tasks in NQR experiments involving systems with 2 and 3 q-bits.

2. Theory

This section provides a brief guide to calculate the dynamics of an ensemble of nuclear spins (possessing nuclear electric quadrupole moment) submitted to static quadrupole plus Zeeman interactions and to a perturbative RF field [10]. By using average Hamiltonian expansion up to second-order, both single- and double-quantum transitions can be excited. Using the density operator formalism, the initial state of thermal equilibrium (in the high-temperature approximation) is given by

$$\rho_{eq} = \frac{1}{Z} \left(\hat{1} - \frac{H_0}{kT} \right), \quad (1)$$

where H_0 is the time-independent Hamiltonian corresponding to the unperturbed system, and Z is the canonical partition function. With application of a time-dependent perturbation, e.g., an RF field described by the Hamiltonian $H_1(t)$, the temporal evolution of the density operator is given by

$$\rho(t) = U(t)\rho(0)U^\dagger(t), \quad (2)$$

where the time-evolution operator U satisfies the equation

$$i\hbar \frac{dU(t)}{dt} = H(t)U(t), \quad (3)$$

with

$$H(t) = H_0 + H_1(t). \quad (4)$$

The explicit time dependence of the operator H makes relatively complicated the solution of Eq. (3). This problem is commonly approached by using the interaction picture [10,11], defined by the transformation

$$\tilde{A}(t) = \exp\left(\frac{iH_0t}{\hbar}\right)A_s(t)\exp\left(\frac{-iH_0t}{\hbar}\right), \quad (5)$$

where A_s and \tilde{A} correspond to the same operator described in the Schrödinger and in the interaction pictures, respectively. In the interaction picture, the dynamics of the system is dictated solely by the perturbation Hamiltonian \tilde{H}_1 . The time dependence of this Hamiltonian in the interaction picture is then removed by using average Hamiltonian theory [41,42]. Keeping the two terms of lowest order in the Magnus expansion [43], we obtain

$$\overline{\tilde{H}_1}^{(0)} = \frac{1}{T} \int_0^T dt' \tilde{H}_1(t'); \quad (6)$$

$$\overline{\tilde{H}_1}^{(1)} = \frac{-i}{2T} \int_0^T dt' \int_0^{t'} dt'' [\tilde{H}_1(t'), \tilde{H}_1(t'')]; \quad (7)$$

where the integration limit T corresponds to the time of application of the perturbation (e.g., the duration of an RF pulse).

Using $\tilde{H}_1 = \tilde{H}_1^{(0)} + \tilde{H}_1^{(1)}$ in Eq. (4), the solution for the time-evolution operator is

$$\tilde{U}(t) = \exp\left(\frac{-i\overline{\tilde{H}_1}t}{\hbar}\right). \quad (8)$$

The density operator at any time t just after the application of the perturbation is then calculated by the expression

$$\tilde{\rho}(t) = \exp\left(\frac{-i\overline{\tilde{H}_1}t}{\hbar}\right)\tilde{\rho}(0)\exp\left(\frac{i\overline{\tilde{H}_1}t}{\hbar}\right). \quad (9)$$

Generally, the dominant Hamiltonian H_0 contains all time-independent interactions affecting the nuclear spin. In the cases of interest for the present discussion, these reduce to Zeeman and quadrupole couplings:

$$H_0 = H_Q + H_Z. \quad (10)$$

These Hamiltonians will be described in terms of a cartesian reference frame, designated as the laboratory system (LAB).

The electric field gradient (EFG) acting on the nuclear site is defined by the tensor $V_{\alpha\beta} = \partial^2V/\partial\alpha\partial\beta$, where α and β are cartesian coordinates and V is the classical electrostatic potential. This tensor is real, symmetric and traceless [11], being thus completely determined by five independent components. In the principal axes system (PAS) of the tensor $V_{\alpha\beta}$ (i.e., in the axes system where the tensor is diagonal), only two components are required, which are conventionally given by the EFG magnitude $eq = V_{ZZ}$ and the asymmetry parameter $\eta = (V_{YY} - V_{XX})/V_{ZZ}$. Therefore, the tensor $V_{\alpha\beta}$ can be described by these two parameters together with the Euler angles that relate the PAS to the LAB system (α_Q, β_Q and γ_Q). Thus, the quadrupole Hamiltonian in the LAB system is given by [11]

$$H_Q = \frac{eQ}{I(2I-1)} \left(\frac{1}{2} (3I_z^2 - \tilde{I}^2) V_{2,0} + \frac{\sqrt{6}}{4} \left((I_z I_+ + I_+ I_z) V_{2,-1} - (I_z I_- + I_- I_z) V_{2,+1} + I_+^2 V_{2,-2} + I_-^2 V_{2,+2} \right) \right), \quad (11)$$

where Q is the nuclear electric quadrupole moment, I is the nuclear spin quantum number, I_z, \tilde{I}, I_+ and I_- are the corresponding spin operators and

$$V_{2,0} = \frac{eq}{2} \left(\frac{3 \cos^2 \beta_Q - 1}{2} + \frac{\eta \sin^2 \beta_Q (e^{2i\gamma_Q} + e^{-2i\gamma_Q})}{4} \right), \quad (12)$$

$$V_{2,\pm 1} = \frac{eq}{2} \left(\mp \sqrt{\frac{3}{8}} \sin 2\beta_Q e^{\pm i\alpha_Q} + \frac{\eta}{\sqrt{6}} \left(-\frac{1 \mp \cos \beta_Q}{2} \sin \beta_Q e^{\pm i(\alpha_Q \mp 2\gamma_Q)} + \frac{1 \pm \cos \beta_Q}{2} \sin \beta_Q e^{i(\pm \alpha_Q + 2\gamma_Q)} \right) \right) \quad (13)$$

and

$$V_{2,\pm 2} = \frac{eq}{2} \left(\sqrt{\frac{3}{8}} (\sin^2 \beta_Q) e^{\pm 2i\alpha_Q} + \frac{\eta}{\sqrt{6}} \left(\frac{(1 \mp \cos \beta_Q)^2}{4} e^{\pm 2i(\alpha_Q \mp \gamma_Q)} + \frac{(1 \pm \cos \beta_Q)^2}{4} e^{2i(\pm \alpha_Q + \gamma_Q)} \right) \right). \quad (14)$$

The quadrupole coupling constant is defined by $C_Q = e^2qQ/h$ (in units of angular frequency).

In the LAB system, the Zeeman Hamiltonian is given by

$$H_Z = -\hbar\omega_L (\sin \theta_Z \cos \phi_Z I_x + \sin \theta_Z \sin \phi_Z I_y + \cos \theta_Z I_z), \quad (15)$$

where θ_Z and ϕ_Z are, respectively, the polar and azimuthal angles of the magnetic field \mathbf{B}_0 with respect to the LAB system, and $\omega_L = \gamma B_0$ is the Larmor frequency.

The time-dependent Hamiltonian H_1 can be written, in general, as the sum of several linearly polarized RF Hamiltonians, according to equation

$$H_1 = \sum_i H_{RF_i}, \quad (16)$$

where

$$H_{RF_i}(t) = -\hbar\omega_{RF_i} \left(\sin \theta_{RF_i} \cos \phi_{RF_i} I_x + \sin \theta_{RF_i} \sin \phi_{RF_i} I_y + \cos \theta_{RF_i} I_z \right) \times \cos(\omega_{RF_i} t - \phi_i), \quad (17)$$

where θ_{RF_i} and ϕ_{RF_i} are, respectively, the polar and azimuthal angles of the oscillating magnetic field \mathbf{B}_{RF_i} with respect to the LAB system, and ω_{RF_i} , ω_{RF_i} and ϕ_i are the amplitude, angular frequency and phase of each RF field, respectively.

All Hamiltonians presented above were defined seeking as greater generality as possible, thus presenting a large number of free parameters. Differently from many programs commonly used for simulation of NMR or NQR experiments, in our approach there is no need to decide beforehand which interaction (Zeeman or quadrupole) is the dominant one. The change to the interaction picture (Eq. (5)) is completely general and allows situations as distinct as zero-field NQR and high-field NMR to be treated within the same theoretical framework. This high degree of freedom facilitates the computational description of a large number of diverse experiments, as described below.

3. Programming interface

The implementation of the equations described in the preceding section is performed using the software Mathematica – version 7.0 [17]. The temporal evolution of the system is obtained by the function **Pulse** $[\rho(0)]$, which returns the density matrix $\rho(t_p)$ after the application of an RF pulse to the initial state $\rho(0)$. The implementation of this function should be performed after defining the parameters **H0**, **H1** and **TP** (the latter corresponding to the duration of the RF pulse). To facilitate the calculation of the matrices **H0** and **H1**, functions were developed to determine the Hamiltonian of the main interactions involved, for any spin value. The function **HQ[spin]** returns the matrix of the quadrupole Hamiltonian, given the parameters **alphaQ**, **betaQ**, **gammaQ**, **cQ** and **eta**.¹ The function **HZ[spin]** returns the matrix of the Zeeman

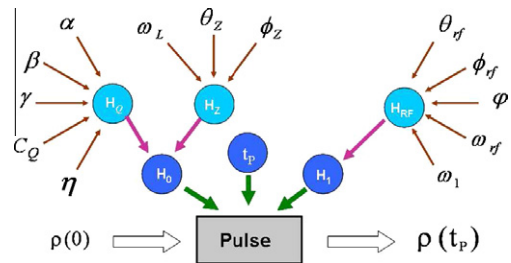


Fig. 1. Diagram illustrating the operation of the main function (**Pulse**) in the developed program.

Hamiltonian, given the parameters **wL**, **thetaZ** and **phiZ**. The function **HRF[spin]** returns the matrix of the Hamiltonian corresponding to a linearly polarized RF pulse, given the parameters **wRF**, **w1**, **phase**, **thetaRF** and **phiRF**. More sophisticated pulses, such as multifrequency pulses or those involving RF fields with elliptical polarization, can be constructed by setting **H1** as an appropriate superposition of functions **HRF[spin]**, according to Eq. (16). This point will be exemplified later. A diagram representing the basic operation of this program is shown in Fig. 1.

Other useful functions for the analysis and simulation of NQR/NMR experiments were also created. The function **Grad** $[\rho(0)]$ returns the state after applying a pulsed magnetic field gradient along the z-axis. The parameters of this function are the pulse duration **TG** and the rate of spatial variation of the magnetic field **G**. The function **FID[rho]** returns a time-dependent oscillating function, representing the free induction decay (FID) measured by a detecting coil placed in a direction determined by the parameters **thetaDet**, **phiDet** (polar and azimuthal angles of the axis of the detecting coil with respect to LAB system, respectively). To include transverse relaxation effects, the parameter **relaxation** (rate of relaxation) must be defined before the application of the function **FID[rho]**. For simplicity, the relaxation rates for all single-quantum coherences are considered identical. Functions **FourierPhase[rho]**, **FourierQuad[rho]** and **FourierAbs[rho]** return, respectively, the real part, imaginary part and absolute value of the Fourier transform of **FID[rho]**, thus allowing the analysis of experiments involving phase-sensitive detection in the frequency-domain. The visualization of the corresponding NMR/NQR spectra and other plots can be easily accomplished by using the usual features available in Mathematica (as exemplified below).

The complete source code of the program here presented is freely available for download [44]. Also included in the referred website are the details (specific source codes, figures, etc.) corresponding to the examples described in the next sections.

4. Examples

This section gives examples of numerical simulation of some typical NMR/NQR experiments, including zero- or low-field NQR and high-field NMR. With these examples, we wish to demonstrate how to use the basic functions of the program, highlighting its versatility, ease of use and broad range of applicability to different types of magnetic resonance experiments involving quadrupolar nuclei.

4.1. Nuclear quadrupole resonance

The first examples discussed here involve the recording of NQR spectra for a system of nuclei with spin 3/2 in an EFG with axial symmetry under a small Zeeman perturbation. This is the case of ³⁵Cl nuclei in KClO₃ and NaClO₃, for example [13,45]. For the pure

¹ The names of all variables used in the source code were chosen as closely as possible to the symbols defined in the preceding section.

```

(* temporal evolution of density operator *)
spin = 3/2;
alphaQ = 0; betaQ = 0; gammaQ = 0; eta = 0; cQ = 2*(2*Pi)*28.1*10^6; (* parameters of the quadrupole interaction *)
wL = 2.0*10^4; thetaZ = 0; phiZ = 0; (* parameters of the Zeeman interaction *)
w1 = 1.0*10^5; wRF=(2*Pi)*28.1*10^6; thetaRF=Pi/2; phiRF=0; phase=0; (* parameters of the RF interaction *)
H0 = HQ[spin]+HZ[spin]; (* non-perturbed Hamiltonian *)
H1 = HRF[spin]; (* RF Hamiltonian *)
TP = 20*10^-6; (* duration of the pulse *)
rho = Pulse[-H0];

(* Fourier transform of the signal detected by a coil in the x-axis *)
thetaOb = Pi/2; phiOb = 0; (* orientation of the detection coil *)
relaxation = 300; (* relaxation rate *)
fourier = FourierAbs[density];

(* plot of the spectrum *)
f = fourier/.w->(1000*(2*Pi)*freq-wRF); (* change of reference frequency *)
Plot[f,{freq,-10,10},
PlotRange->All, Axes->None,
FrameLabel->"kHz", Frame->{{False,False},{True,False}}]

```

(a)

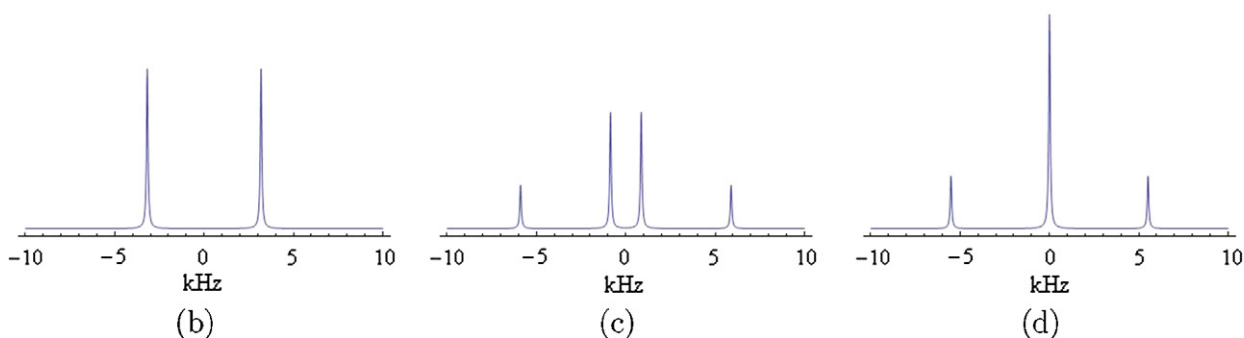


Fig. 2. (a) Source code for the simulation of ^{35}Cl NQR spectra in a single crystal of KClO_3 . The symmetry axis of the EFG tensor is defined as the z -axis. The RF field is linearly polarized along the x -axis, near resonance ($\omega_{\text{RF}} = \omega_Q$). The detection is performed with the same coil used for excitation ($\theta_{\text{Det}} = \theta_{\text{RF}}$ and $\phi_{\text{Det}} = \phi_{\text{RF}}$). The static magnetic field is small ($\omega_L \ll \omega_Q$) and the angle it makes with the EFG symmetry axis is $\theta_Z = 0$ (b), $\theta_Z = \pi/4$ (c) or $\theta_Z = \arctan \sqrt{2}$ (d).

quadrupole Hamiltonian, the states $\pm 3/2$ are degenerate, as well as the states $\pm 1/2$, so that the NQR spectrum contains only a single line at a frequency in the range 28–29 MHz. A small Zeeman field (~ 10 G) causes a frequency splitting (of a few kHz) and make the first-order corrected eigenvectors as linear superpositions of angular momentum eigenvectors [13]. The number, position and intensity of these lines are dependent on the angle θ_Z between the static magnetic field and the EFG symmetry axis. This problem can then be completely understood by using stationary first-order perturbation theory and it serves as a good example to illustrate the operation of our simulation program.

Potassium chlorate (KClO_3) has a monoclinic structure, with two molecules per unit cell. The symmetry axes of the EFG tensors at the ^{35}Cl nuclei of each molecule are parallel to one another, so that these molecules behave identically for any direction of the externally applied static magnetic field [45]. Fig. 2a shows a source code for simulation of the ^{35}Cl NQR spectrum in a single crystal of KClO_3 ($\omega_Q/2\pi = 28.1$ MHz). Fig. 2b–d shows three simulated spectra obtained for three different values of θ_Z . These spectra can be directly compared to experimental results long known in the NQR literature [13,45].

Sodium chlorate (NaClO_3) possesses cubic structure, with four molecules per unit cell, all with the same ^{35}Cl NQR frequency ($\omega_Q/2\pi = 29.93$ MHz). However, unlike KClO_3 , the symmetry axes

of the EFG tensors at the ^{35}Cl nuclei corresponding to these four molecules are not parallel to each other; instead, they are parallel to each of the diagonals of the unit cell cube [13,45]. For a given direction of the externally applied static magnetic field, there will be four angles between this field and each of the EFG symmetry axes (some of which can coincide). Thus, each crystallographically distinct site must be treated separately. For the numerical simulation, one should proceed similarly to the previous example for each site and add the results in the end (either in the time or in the frequency domain). This problem is handled in the source code [44] by keeping the static magnetic field fixed at a given direction (common to all sites) and specifying the angular parameters of the quadrupole interaction for each site ($\alpha_Q = \pi/4, 3\pi/4, 5\pi/4$ or $7\pi/4$; $\beta_Q = \arctan \sqrt{2}$ and $\gamma_Q = 0$ for all sites). In general, the spectrum has 16 lines (four for each distinct site), but for some specific orientations of the magnetic field there can be some coincidence in the angles between the magnetic field and the EFG symmetry axes. Thus, the number of observed lines can be reduced [13,45], as illustrated in the simulated spectra shown in Fig. 3.

We now turn to a more sophisticated NQR experiment, involving two-photon transitions. The occurrence of these transitions can be understood by using average Hamiltonian theory up to the first-order term in the Magnus expansion. Two-photon excitation occurs in general with two RF fields whose frequencies sum to or

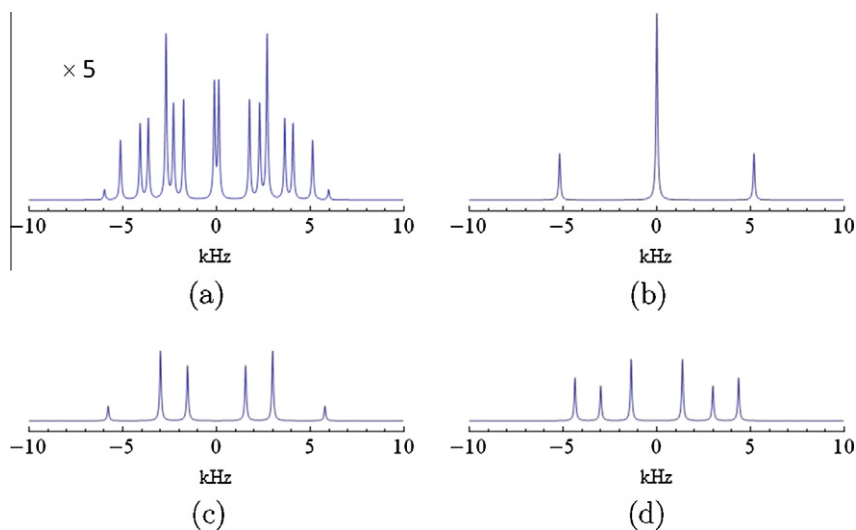


Fig. 3. Simulation of Zeeman-perturbed ^{35}Cl NQR spectra of NaClO_3 single crystal: (a) $\theta_z = \pi/4$ and $\phi_z = \pi/3$; (b) $\theta_z = 0$ and $\phi_z = 0$; (c) $\theta_z = \pi/4$ and $\phi_z = 0$ and (d) $\theta_z = \arctan \sqrt{2}$ and $\phi_z = \pi/4$. The other parameters are the same as in Fig. 2a.

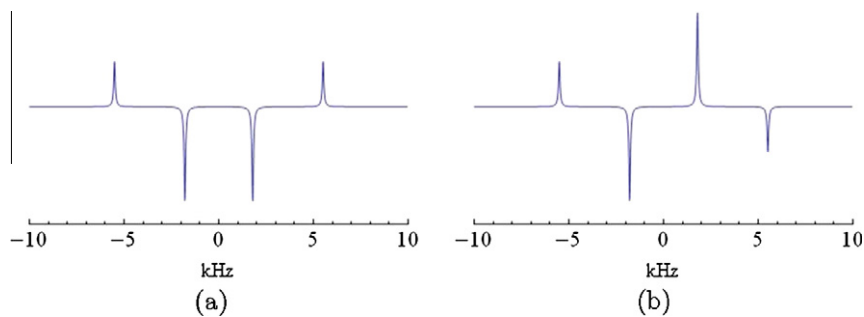


Fig. 4. Simulation of Zeeman-perturbed ^{35}Cl NQR spectra of KClO_3 with two-photon excitation. The symmetry axis of the EFG tensor is defined as the z -axis. An external magnetic field of 8 G was applied with $\theta_z = \pi/6$. (a) Detection with a coil perpendicular to the excitation coil ($\theta_{RF} = \theta_{Det} = \pi/2$; $\phi_{RF} = \phi_{Det} + \pi/2$). (b) Detection with the same excitation coil ($\theta_{RF} = \theta_{Det} = \pi/2$; $\phi_{RF} = \phi_{Det}$).

differ by the resonance frequency [42]. Eles & Michal demonstrated the two-photon excitation in ^{35}Cl NQR of NaClO_3 and KClO_3 single crystals using RF pulses applied at half the NQR frequency. Signals due to both, single- and double-quantum coherences were detected, with application of a small static magnetic field. This experiment can be easily simulated with the program presented in this work, using input parameters similar to the ones given in Fig. 2a, but setting $\omega_{RF} = \omega_Q/2$ (i.e., excitation at half the NQR frequency). Two examples of simulated spectra obtained with two-photon excitation are given in Fig. 4. These spectra can be compared to the experimental results given in Fig. 6 of Ref. [19].

4.2. High-field NMR

As mentioned above, one of the most useful features of the program presented here is its versatility, allowing that similar procedures can be used for simulation of NQR (where the quadrupole interaction is dominant), or high-field NMR experiments (where the Zeeman interaction is dominant) or even in cases where both interactions have comparable magnitude. As an example of simulation of high-field NMR spectrum of a quadrupolar nucleus, Fig. 5 presents the simulated ^{23}Na NMR spectrum of NaClO_3 single crystal [46]. In this case, each crystallographically inequivalent ^{23}Na nucleus gives rise to a triplet, with the central transition (between the states $\pm 1/2$, which is not affected by the quadrupole

interaction to first-order) flanked by two satellites. As there are four molecules per unit cell in this crystal, the spectrum shows a strong central line (consisting of the superposition of the four central transitions) and four pairs of satellites. An experimental spectrum to be compared with this simulation can be found in Fig. 3 of Ref. [46].

Another quite interesting example dealing with spin dynamics of quadrupolar nuclei in high-field NMR was provided very

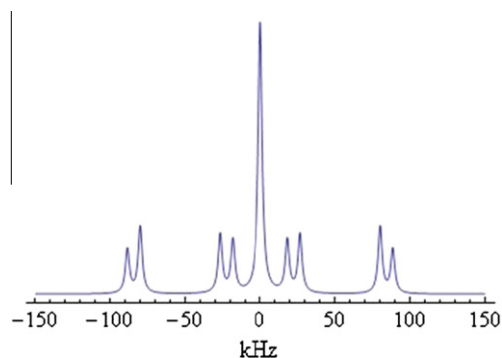


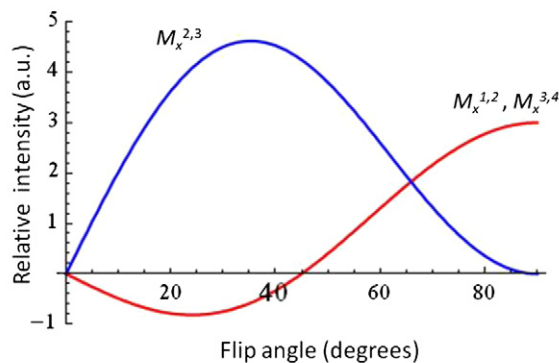
Fig. 5. Simulation of high-field ^{23}Na NMR spectrum of NaClO_3 single crystal. The quadrupole coupling constant is approximately 0.80 MHz and the Larmor frequency is 132 MHz.

```

spin = 3/2;
(* parameters of the non-perturbed interaction *)
vL = 2 * Pi * 79.46 * 10^6; thetaZ = 0; phiZ = 0;
alpha0 = 0; beta0 = 0; gamma0 = 0; eta = 0; cQ = 2 * (2 * Pi * 51.0 * 10^3);
H0 = H0[spin] + HZ[spin];
(* parameters of the RF interaction *)
vRF = vL; w1 = Pi/(2*10^-6); thetaRF = Pi/2; phiRF = 0; phase = Pi/2;
H1 = HRF[spin];
(* matrices of fictitious spin 1/2 operators *)
I12 = {{0,1/2,0,0}, {1/2,0,0,0}, {0,0,0,0}, {0,0,0,0}};
I23 = {{0,0,0,0}, {0,0,1/2,0}, {0,1/2,0,0}, {0,0,0,0}};
I34 = {{0,0,0,0}, {0,0,0,0}, {0,0,0,1/2}, {0,0,1/2,0}};
(* determining the initial state *)
rho0 = {{1,0,0,0},{0,3,0,0},{0,0,-3,0},{0,0,0,-1}};
(* calculation of relative intensity versus flip angle *)
NumPoints = 30; PlotMax = 90;
M12 = Table[{0,0},{NumPoints+1}]; M23 = Table[{0,0},{NumPoints+1}]; M34 = Table[{0,0},{NumPoints+1}];
Do[flip = i * (PlotMax/NumPoints); TP = (flip/90) * (2 * 10^-6);
  rho1 = Pulse[rho0];
  j12 = ((MatrixExp[(-I*H0*TP)/hbar].I12.MatrixExp[(I*H0*TP)/hbar]));
  j23 = ((MatrixExp[(-I*H0*TP)/hbar].I23.MatrixExp[(I*H0*TP)/hbar]));
  j34 = ((MatrixExp[(-I*H0*TP)/hbar].I34.MatrixExp[(I*H0*TP)/hbar]));
  M12[[i+1]] = {flip,Sqrt[3]*Tr[rho1.j12]};
  M23[[i+1]] = {flip,2*Tr[rho1.j23]};
  M34[[i+1]] = {flip,Sqrt[3]*Tr[rho1.j34]},
  {i,1,NumPoints}]
(* plot results *)
ListPlot[{M12,M23,M34},PlotRange->{-1,5},TicksStyle->Directive[20],PlotJoined->True,PlotStyle->Thick]

```

(a)



(b)

Fig. 6. Source code (a) and simulated results (b) corresponding to the flip angle dependence of the intensities of satellite and central transitions for spin 3/2 nuclei in a single crystal, starting with the populations associated with both satellite transitions inverted and with non-selective excitation of the spectrum.

recently by Nakashima et al., who described the pulse response of half-integer spin quadrupolar nuclei in single crystals starting from general initial states (not necessarily corresponding to thermal equilibrium) [47]. This subject is of high interest considering the many sensitivity enhancement methods currently used for half-integer spin quadrupolar nuclei that are based upon population transfers. Most of these methods involve the saturation or inversion of satellite transitions (achieved by pulse trains or by adiabatic inversion pulses), which leads to an enhanced population difference for the selectively excited/observed central transition [48–51]. Nakashima et al. studied the effect of observe pulse flip angle on the intensities of the satellite and central transitions in NMR of quadrupolar nuclei in single crystals, using non-selective excitation and starting from non-equilibrium initial states. The populations corresponding to the satellite transitions were inverted using hyperbolic secant (HS) pulses. Such results can be easily simulated using the program presented in this work, by starting from an initial density operator with inverted populations corresponding to the satellite transitions. For spin 3/2, the x -magnetization

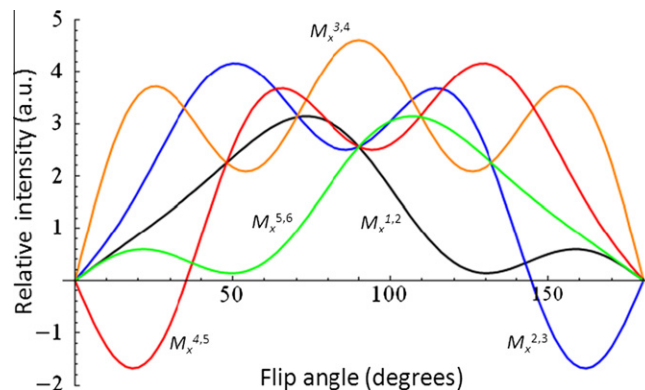


Fig. 7. Simulated intensity plots for the flip angle dependence of the intensity of each of the several transitions for spin 5/2 nuclei in a single crystal, starting with the consecutive inversion of the populations of the two satellite transitions at one side of the central transition and with non-selective excitation of the spectrum.

```

wq=63460; (* quadrupole frequency *)
rho0=-H0; (* equilibrium state *)
vRF=(2*wL-wq)/2; TP=0.5*10^-3; w1=15172; H1=HRF[spin]; rho1=Pulse[rho0]; (* double quantum pulse *)
vRF=(wL+wq); TP=0.5*10^-3; w1=7250; H1=HRF[spin]; rho2=Pulse[rho1]; (* single quantum pulse *)
G=250*10^-4; TG=1.0*10^-3; rho3=Grad[rho2]; (* magnetic field gradient *)
vRF=wL; TP=1.0*10^-6; w1=(Pi/20)/TP; H1=HRF[spin]; rho4=Pulse[rho3]; (* detection pulse *)

```

(a)

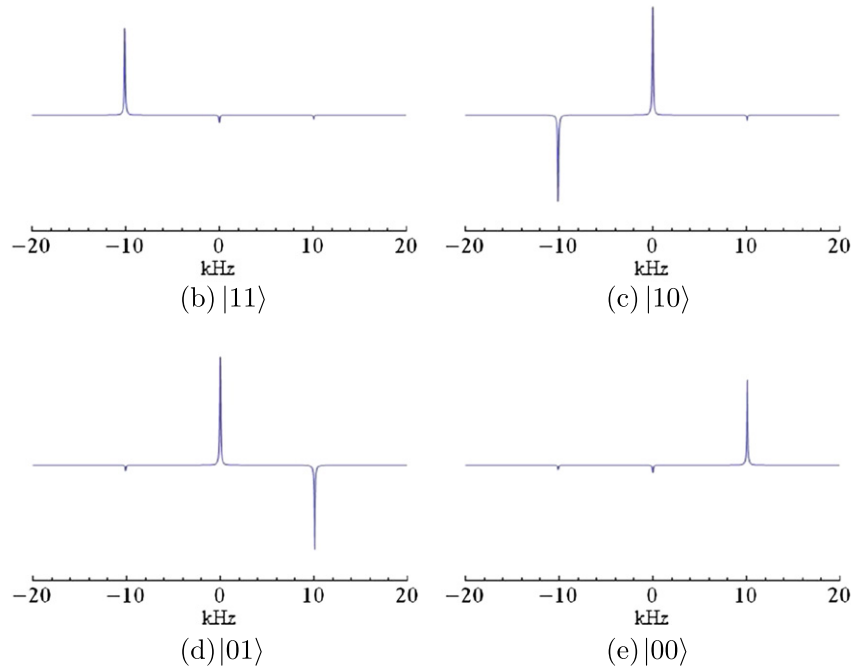


Fig. 8. (a) Source code excerpt used to implement the pulse sequence that generates the pseudopure state $|01\rangle$ in a 2 q-bit system associated with high-field ^{23}Na NMR in a liquid crystal. (b)–(e) Simulated ^{23}Na NMR spectra for the four pseudopure states of the computational basis. The numerical values of the experimental parameters were taken from [26].

can be decomposed into three components, referring to the two satellite transitions $M_x^{1,2}$ and $M_x^{3,4}$ and to the central transition $M_x^{2,3}$, and can be calculated in terms of fictitious spin-1/2 operators I_x^{fs} [52,53] by equations

$$\langle M_x^{1,2}(t) \rangle \propto \text{Tr}(\rho(t)\sqrt{3}I_x^{1,2}(t)), \quad (18)$$

$$\langle M_x^{2,3}(t) \rangle \propto \text{Tr}(\rho(t)2I_x^{2,3}(t)), \quad (19)$$

and

$$\langle M_x^{3,4}(t) \rangle \propto \text{Tr}(\rho(t)\sqrt{3}I_x^{3,4}(t)). \quad (20)$$

Fig. 6a shows the complete code to perform the simulation of the flip angle dependence of the ^{23}Na NMR intensities in NaNO_3 single crystal. The initial state was constructed by inverting the populations of states $|3/2\rangle$ and $|1/2\rangle$, as well as those of states $|-3/2\rangle$ and $|-1/2\rangle$; the system was excited by a non-selective RF pulse with $\omega_{RF} = \omega_L$, for various values of t_p (or flip angle). The simulation result is shown in Fig. 6b, which can be compared to the calculations and experimental results shown in Fig. 3 of reference [47]. A similar analysis can be performed for spin 5/2 nuclei, as done by Nakashima et al. using ^{27}Al NMR measurements in a single crystal of Al_2O_3 . Fig. 7 shows the result of our simulations, which can be directly compared to the calculations shown in Fig. 6 of reference [47]. The initial state was obtained by inversion of the populations of states $|-5/2\rangle$ and $|-3/2\rangle$, followed by inversion of the populations of states $|-3/2\rangle$ and $|-1/2\rangle$. All procedures to perform the simulation are similar to the previous example.

4.3. Quantum computing by NMR

The examples discussed so far involved the use of single and non-selective RF pulses. The examples presented in this section show how to simulate experiments making use of more elaborated pulse sequences, which can be non-selective (“hard”) or selective (“soft”). The use of these pulse sequences is especially important in the context of quantum computing, where precise manipulation of populations and coherences in the density operator is required.

Quantum computing involves the handling of quantum systems to perform data processing tasks. In NMR, this is accomplished through the application of specific RF pulses (logic gates) on ensemble states adequately prepared, called pseudopure states [20]. These states are characterized by having all populations in their respective density operators equalized, except for one, while all coherences are zero. In the next examples, we shall monitor the achievement of pseudopure states and application of basic logic gates for systems of quadrupolar nuclei.

Khitrin & Fung showed how to obtain pseudopure states in a 2 q-bit system, using high-field ^{23}Na NMR (spin = 3/2) in a liquid crystal [26]. The equalization of the populations was achieved through a sequence of selective RF pulses exciting either single- or double-quantum transitions. Undesirable coherences were eliminated by applying pulsed magnetic field gradients. The signal was detected after application of a hard reading pulse ($\pi/20$). All these steps can be implemented in our simulation program by successive application of the function **Pulse**, as exemplified in the source code shown in Fig. 8a. The simulated spectra associated

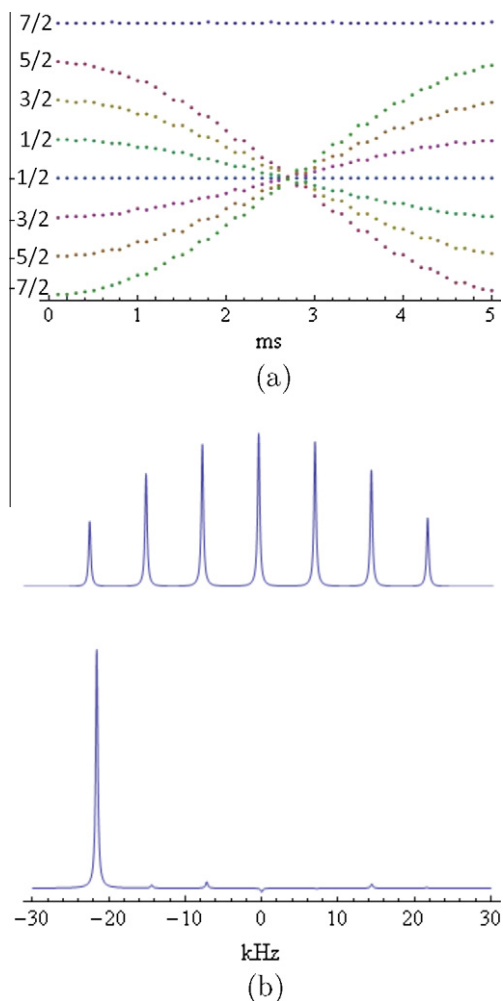


Fig. 9. (a) Simulation of the evolution of populations in a high-field NMR experiment for a nucleus with spin 7/2 (3 q-bit system) following a multifrequency pulse. For $t_p \approx 2.7$ ms all populations are equalized, except the one corresponding to $m = 7/2$, which corresponds to the pseudopure state $|000\rangle$. (b) Simulated ^{133}Cs NMR spectra corresponding to thermal equilibrium (above) and to the pseudopure state $|000\rangle$ (below).

with the four pseudopure states are exhibited in Fig. 8b–e. The corresponding experimental spectra can be found in Fig. 2 of Ref. [26].

In another study, Khitritin et al. [27] obtained pseudopure states for a 3 q-bit system using ^{133}Cs NMR (spin = 7/2) in a liquid crystal under strong magnetic field. In this case the experiments employed multifrequency RF pulses, so that all population changes were achieved simultaneously, providing a considerable time saving. Multifrequency pulses can be implemented in the program here described by defining separately the Hamiltonians for each RF frequency and setting H_1 as the sum of them all (see Eq. (16)). To create the pseudopure state associated with $m = 7/2$, for example, the equalization of all other populations is achieved with a single pulse consisting of the superposition of the six harmonics corresponding to the six transition frequencies $\omega_{12}, \omega_{23}, \omega_{34}, \omega_{45}, \omega_{56}$ and ω_{67} , with amplitudes proportional to 0.81, 0.93, 1, 1.03, 1.04 and 1.06, respectively. The optimum duration of this pulse (TP) can be obtained following the dynamics of population changes, as shown in the plot exhibited in Fig. 9a, which was constructed using our program features; a similar plot, obtained using other simulation procedures, was also presented in Fig. 2 of Ref. [27]. After this multifrequency pulse, a pulsed magnetic field gradient is used to eliminate the coherences, leading to the desired pseudopure state (Fig. 9(b)).

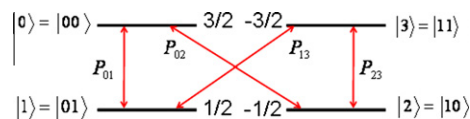


Fig. 10. Energy level diagram for a spin 3/2 nucleus coupled to an axially symmetric EFG, with zero applied magnetic field (pure NQR). The selective pulses defined in Table 1 are indicated.

Table 1

Designation of selective pulses for a system of spin 3/2 nuclei in pure NQR.

Single quantum			Double quantum		
Pulse	Helicity	Frequency (ω_Q)	Pulse	Helicity	Frequency (ω_Q)
P_{01}	+	1	P_{02}	+	0.5
P_{23}	-	1	P_{13}	-	0.5

4.4. Quantum computing by NQR

The examples given in this subsection deal with the use of NQR for implementation of ensemble quantum computing, following in general terms the methods well established in high-field NMR [20] but adapting all procedures to the different dynamics involved in NQR experiments. These examples constitute original proposals for creation of pseudopure states and implementation of logic gates in systems where the dominant interaction is the quadrupole coupling between a nucleus with spin $>1/2$ and an axially symmetric EFG. The manipulation of the ensemble quantum states is achieved by using selective RF pulses with circular polarization. In fact, the use of circularly polarized RF provides a mechanism for selective excitation in NQR with no analogous in high-field NMR. An RF pulse with circular polarization around the z-axis can be described by the sum of two linearly polarized Hamiltonian terms, according to equation

$$H_1^\pm(t) = -\hbar\omega_1 I_x \cos \omega_{RF}t - \hbar\omega_1 I_y \cos \left(\omega_{RF}t \pm \frac{\pi}{2} \right). \quad (21)$$

In keeping with the principle of conservation of angular momentum, H_1^+ excites only transitions with increasing z-component ($\Delta m > 0$), while H_1^- excites only transitions with $\Delta m < 0$.

In pure NQR (i.e., with no applied magnetic field) of a system of spin 3/2 nuclei coupled to an axially symmetric EFG, such as ^{35}Cl nuclei in KClO_3 single crystal, the levels $\pm 3/2$ are degenerate, as well as the levels $\pm 1/2$, so that the frequencies of single-quantum transitions ($3/2 \leftrightarrow 1/2$ and $-3/2 \leftrightarrow -1/2$) are identical; the same applies to the double-quantum transitions ($3/2 \leftrightarrow -1/2$ and $-3/2 \leftrightarrow 1/2$), as shown Fig. 10. However, these transitions can be distinguished (and selectively excited/detected) by using RF pulses circularly polarized around the symmetry axis of the EFG, due to differences in Δm signs. The use of circularly or, more generally, elliptically polarized RF pulses has been widespread in NQR experiments, especially with the aim of achieving selective excitation or increasing sensitivity [39,40,54]. These RF fields can be generated using crossed coils or birdcage resonators, as it is usual in magnetic resonance imaging [18,40,55].

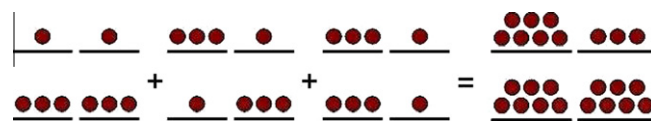


Fig. 11. Schematic population diagram representing the creation of the pseudopure state $|11\rangle$ for a system of spin 3/2 nuclei in pure NQR.

```

spin = 3/2;
wq = (2*Pi)*28.1*10^6;
alphaQ = 0; betaQ=0; gammaQ=0; eta=0; cQ=2*wq;
H0 = HQ[spin];

    rhoEq = H0; (* equilibrium *)

w1 = wq/1000; thetaRF = Pi/2; vRF = wq;
phiRF = 0; phase = 0; hx = HRF[spin];
phiRF = Pi/2; phase = Pi/2; hy = HRF[spin];
H1 = hx + hy;
TP = Pi/(Sqrt[3] * w1);
    rhoS = Pulse[H0]; (*single quantum*)

w1 = wq/1000; thetaRF = Pi/2; vRF = wq/2;
phiRF = 0; phase = 0; hx = HRF[spin];
phiRF = Pi/2; phase = Pi/2; hy = HRF[spin];
H1 = hx + hy;
TP = Pi*wq/(2*Sqrt[3]*w1^2);
    rhoD = Pulse[H0]; (*double quantum*)

rho11 = ( rhoEq + rhoS + rhoD ); (* pseudopure state 11 *)

```

Fig. 12. Source code for simulating the experiment for creation of the pseudopure state $|11\rangle$ in the case of a system of spin $3/2$ nuclei in pure NQR.

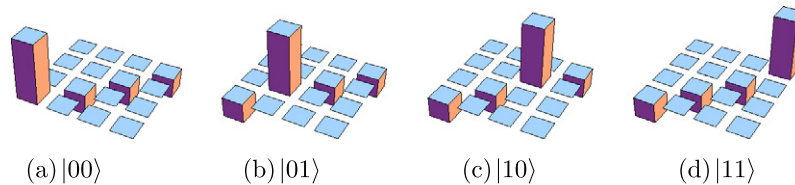


Fig. 13. Real part of the density matrices corresponding to the four pseudopure states of the computational basis, obtained by numerical simulation, in the case of a system of spin $3/2$ nuclei in pure NQR.

In the case of spin $3/2$ nuclei, the single-quantum transitions are excited using on-resonance pulses ($\omega_{RF} = \omega_Q$), whereas the double-quantum transitions are obtained by excitation at half the resonance frequency ($\omega_{RF} = \omega_Q/2$) [19]. The selective pulses are defined in Table 1. This 4-level system can be used to simulate a system of 2 q-bits, defined by: $|3/2\rangle = |0\rangle = |00\rangle$; $|1/2\rangle = |1\rangle = |01\rangle$; $|-1/2\rangle = |2\rangle = |10\rangle$; $|-3/2\rangle = |3\rangle = |11\rangle$.

Pseudopure states for this system can be obtained by a procedure of temporal averaging, similarly to what is done in high-field NMR experiments [56,57]. The pseudopure state $|3\rangle = |11\rangle$, for example, can be obtained by adding the density operators resulting from three different experiments, as shown below:

$$\rho_3 = \rho_{eq} + P_{01}(\pi) \cdot \rho_{eq} + P_{02}(\pi) \cdot \rho_{eq}. \quad (22)$$

The first term in the sum above is simply the thermal equilibrium state; the second and third ones are obtained from the equilibrium state by application of the inversion pulses P_{01} and P_{02} , respectively. A diagram showing schematically the changes in populations of the energy levels resulting from each step in the above sequence is shown in Fig. 11. The source code to simulate this experiment is given in Fig. 12. The other pseudopure states can be obtained by methods similar to Eq. (22), just by changing appropriately the

polarization state of each pulse. Fig. 13 shows the density matrices corresponding to the four pseudopure states obtained following this method, as simulated using source codes similar to the one given in Fig. 12. Single q-bit rotations can also be implemented by using selective single- and double-quantum RF pulses. The C-Not gate with control on the first q-bit (i.e., an operation that inverts the second q-bit if and only if the first q-bit is 1) is achieved by the single-quantum pulse $P_{23}(\pi)$. On the other hand, the C-Not gate with control on the second q-bit is given by the double-quantum pulse $P_{13}(\pi)$.

Our last example shows how to obtain a pseudopure state in a 3 q-bit system using pure NQR, in an ensemble of spin $7/2$ nuclei subjected to an axially symmetric EFG. The population diagrams corresponding to the thermal equilibrium state and to a pseudopure state are shown in Fig. 14. The respective frequencies and helicities of the selective pulses for this system are defined in Table 2. Pseudopure states can be obtained by a sequence of selective pulses followed by a pulsed magnetic field gradient G . As an example, the state $|0\rangle = |000\rangle$ is obtained by the following sequence S :

$$S = P_{57}(\pi) \cdot P_{35}(\arccos(1/3)) \cdot P_{12}(\pi/2) \cdot P_{45}(\pi/2) \cdot P_{67}(\pi/2) \cdot G. \quad (23)$$

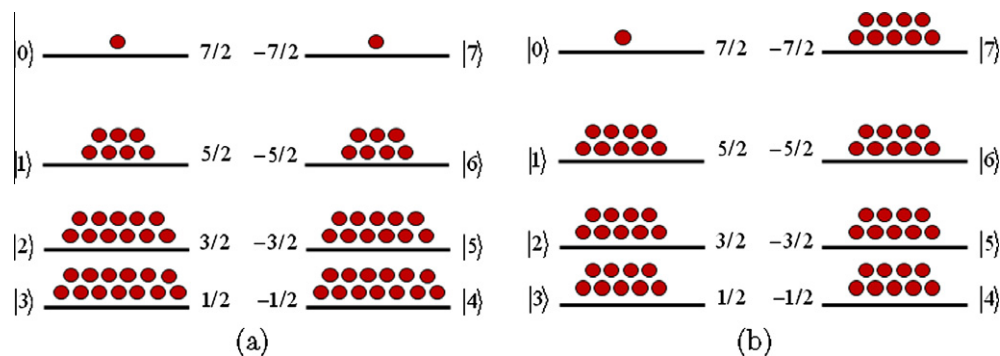


Fig. 14. Schematic population diagram representing (a) the thermal equilibrium state and (b) the pseudopure state $|000\rangle$, obtained by the pulse sequence given in Eq. (23), in the case of a system of spin $7/2$ nuclei in pure NQR.

Table 2
Designation of selective pulses for a system of spin $7/2$ nuclei in pure NQR.

Single quantum			Double quantum		
Pulse	Helicity	Frequency (ω_Q)	Pulse	Helicity	Frequency (ω_Q)
P_{01}	+	3	P_{02}	+	2.5
P_{12}	+	2	P_{13}	+	1.5
P_{23}	+	1	P_{24}	+	0.5
P_{45}	–	1	P_{35}	–	0.5
P_{56}	–	2	P_{46}	–	1.5
P_{67}	–	3	P_{57}	–	2.5

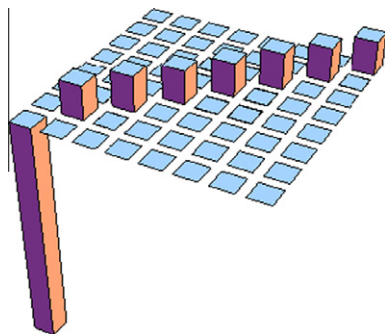


Fig. 15. Real part of the density matrix corresponding to the pseudopure state $|000\rangle$, obtained by numerical simulation, in the case of a system of spin $7/2$ nuclei in pure NQR.

Different from the procedure used in the previous example, here we do not use time averaging; instead, spatial averaging is provided by applying the pulsed magnetic field gradient, which also leads to zero first-order coherences [22]. The density matrix corresponding to the pseudopure state obtained following the sequence S above is shown in Fig. 15, as simulated using the program presented in this work; the other pseudopure states can be prepared by similar procedures.

5. Conclusions

The various examples discussed above show the usefulness and versatility of the simulation program for NQR/NMR experiments presented here. First, several examples of Zeeman-perturbed NQR as well as quadrupole-perturbed high-field NMR experiments were addressed, involving single- and double-quantum transitions, multifrequency pulses, circularly polarized RF pulses and other features. Finally, the last examples presented original proposals for implementation of quantum computing using pure NQR in systems

of nuclei with spin $3/2$ or $7/2$ (corresponding to 2 or 3 q-bits, respectively). These results show that NQR can indeed be useful as a low-cost and easy experimental technique for demonstration of simple quantum computing tasks and simulations of small quantum systems. Both proposals made use of circularly polarized RF pulses and single- and double-quantum transitions, which were straightforwardly simulated using the program here presented. The experimental implementation of these methods is in progress, involving especially designed RF probes with capability of excitation and detection of circularly polarized RF.

Acknowledgments

This work was supported by Brazilian agencies CAPES and CNPq/INCT-IQ. The authors also acknowledge the constructive suggestions of an anonymous reviewer.

References

- [1] M. Bak, J.T. Rasmussen, N.C. Nielsen, SIMPSON: a general simulation program for solid-state NMR spectroscopy, *J. Magn. Reson.* 147 (2000) 296–330.
- [2] S.A. Smith, T.O. Levante, B.H. Meier, R.R. Ernst, Computer simulations in magnetic resonance. An object oriented programming approach, *J. Magn. Reson.* 106 (1994) 75–105.
- [3] W. Studer, SMART, a general purpose pulse experiment simulation program using numerical density matrix calculations, *J. Magn. Reson.* 77 (1988) 424–438.
- [4] A. Jerschow, MathNMR: spin and spatial tensor manipulations in Mathematica, *J. Magn. Reson.* 176 (2005) 7–14.
- [5] P. Hodgkinson, L. Emsley, Numerical simulation of solid-state NMR experiments, *Prog. Nucl. Magn. Reson. Spectrosc.* 36 (2000) 201–239.
- [6] M. Eden, Computer simulations in solid-state NMR. I. Spin dynamics theory, *Concepts Magn. Reson. Part A* 17 (2003) 117–154.
- [7] I. Rodriguez, J. Ruiz-Cabello, Density matrix calculations in MathematicaTM, *Concepts Magn. Reson. Part A* 13A (2003) 143–147.
- [8] M. Goldman, *Quantum Description of High-Resolution NMR in Liquids*, Clarendon Press, Oxford, 1988.
- [9] M.H. Levitt, *Spin Dynamics*, John Wiley & Sons, 2001.
- [10] J. Sakurai, *Modern Quantum Mechanics*, Addison Wesley Longman, 1994.
- [11] C.P. Slichter, *Principles of Magnetic Resonance*, Springer-Verlag, 1990.
- [12] R.R. Ernst, G. Bodenhausen, A. Wokaun, *Principles of Nuclear Magnetic Resonance in One and Two Dimensions*, Oxford, 1987.
- [13] T.P. Das, E.L. Hahn, *Nuclear Quadrupole Resonance Spectroscopy*, Academic Press Inc, 1958.
- [14] E. Harel, C.A. Herman, General numerical analysis of time-domain NQR experiments, *J. Magn. Reson.* 183 (2006) 308–314.
- [15] M.S. Krishnan, F.P. Temme, B.C. Sanctuary, Theory of pulses in nuclear quadrupole resonance spectroscopy, *Molec. Phys.* 78 (1993) 1385–1404.
- [16] D.J. Isbister, M.S. Krishnan, B.C. Sanctuary, Use of computer algebra for the study of quadrupole spin systems, *Molec. Phys.* 86 (1995) 1517–1535.
- [17] Wolfram Research. Mathematica, 2010. <<http://www.wolfram.com>>.
- [18] P.T. Eles, C.A. Michal, Two-photon excitation in nuclear quadrupole resonance, *Chem. Phys. Lett.* 376 (2003) 268–273.
- [19] P.T. Eles, C.A. Michal, Crossed-coil detection of two-photon excited nuclear quadrupole resonance, *J. Magn. Reson.* 175 (2005) 201–209.
- [20] I.S. Oliveira, T.J. Bonagamba, R.S. Sarthour, J.C.C. Freitas, E.R. de Azevedo, *NMR Quantum Information Processing*, Elsevier, 2007.

- [21] M.A. Nielsen, E. Knill, R. Laflamme, Complete quantum teleportation using nuclear magnetic resonance, *Nature* 396 (1998) 52–55.
- [22] I.L. Chuang, N. Gershenfeld, M.G. Kubinec, D.W. Leung, Bulk quantum computation with nuclear-magnetic-resonance: theory and experiment, *Proc. Roy. Soc. Lond. A* 454 (1998) 447–467.
- [23] L.M.K. Vandersypen, M. Steffen, G. Breyta, C.S. Yannoni, M.H. Sherwood, I.L. Chuang, Experimental realization of Shor's quantum factoring algorithm using nuclear magnetic resonance, *Nature* 414 (2001) 883–887.
- [24] D. Gershenfeld, I.L. Chuang, Bulk spin resonance quantum computation, *Science* 275 (1997) 350–356.
- [25] D.G. Cory, A.F. Fahmy, T.F. Havel, Ensemble quantum computing by NMR spectroscopy, *Proc. Natl. Acad. Sci.* 94 (1997) 1634–1639.
- [26] A.K. Khitrin, B.M. Fung, Nuclear magnetic resonance quantum logic gates using quadrupolar nuclei, *J. Chem. Phys.* 112 (2000) 6963–6965.
- [27] A.K. Khitrin, H. Sun, B.M. Fung, Method of multifrequency excitation for creating pseudopure states for NMR quantum computing, *Phys. Rev. A* 63 (2001) 20301.
- [28] G.M. Leskowitz, N. Ghaderi, R.A. Olsen, L.J. Mueller, Three-qubit nuclear magnetic resonance quantum information processing with a single-crystal solid, *J. Chem. Phys.* 119 (2003) 1643–1649.
- [29] F.A. Bonk, R.S. Sarthour, E.R. de Azevedo, J.D. Bulnes, G.L. Mantovani, J.C.C. Freitas, T.J. Bonagamba, A.P. Guimarães, I.S. Oliveira, Quantum-state tomography for quadrupole nuclei and its application on a two-qubit system, *Phys. Rev. A* 69 (2004) 042322.
- [30] F.A. Bonk, E.R. de Azevedo, R.S. Sarthour, J.D. Bulnes, J.C.C. Freitas, A.P. Guimarães, I.S. Oliveira, T.J. Bonagamba, Quantum logical operations for spin 3/2 quadrupolar nuclei monitored by quantum state tomography, *J. Magn. Reson.* 175 (2005) 226–234.
- [31] H. Kampermann, W.S. Veeman, Characterization of quantum algorithms by quantum process tomography using quadrupolar spins in solid-state nuclear magnetic resonance, *J. Chem. Phys.* 122 (2005) 214108.
- [32] J. Teles, E.R. de Azevedo, R. Auccaise, R.S. Sarthour, I.S. Oliveira, T.J. Bonagamba, Quantum states tomography for quadrupolar nuclei using global rotations of the spin system, *J. Chem. Phys.* 126 (2007) 154506.
- [33] T. Gopinath, A. Kumar, Implementation of controlled phase shift gates and Collins version of Deutsch–Jozsa algorithm on a quadrupolar spin-7/2 nucleus using non-adiabatic geometric phases, *J. Magn. Reson.* 193 (2008) 168–176.
- [34] D. Suter, T.S. Mahesh, Spins as qubits: quantum information processing by nuclear magnetic resonance, *J. Chem. Phys.* 128 (2008) 052206.
- [35] L.P. Pryadko, P. Sengupta, Second-order shaped pulses for solid-state quantum computation, *Phys. Rev. A* 78 (2008) 032336.
- [36] J. Lee, A.K. Khitrin, Projection of a quantum state on eigenstates of average Hamiltonian, *J. Magn. Reson.* 198 (2009) 248–251.
- [37] J.A. Jones, Quantum computing with NMR, *Prog. Nucl. Magn. Reson. Spectrosc.* (in press), doi:10.1016/j.pnmrs.2010.11.001.
- [38] G.B. Furman, S.D. Garen, V.M. Meerovich, V.L. Sokolovsky, Two qubits in pure nuclear quadrupole resonance, *J. Phys.: Condens. Matter* 14 (2002) 8715–8723.
- [39] Y.K. Lee, H. Robert, D.K. Lathrop, Circular polarization excitation and detection in ^{14}N NQR, *J. Magn. Reson.* 148 (2001) 255–362.
- [40] J.B. Miller, B.H. Suits, A.N. Garroway, Circularly polarized RF magnetic fields for spin-1 NQR, *J. Magn. Reson.* 151 (2001) 228–234.
- [41] U. Haeblerlen, J.S. Waugh, Coherent averaging effects in magnetic resonance, *Phys. Rev.* 175 (1968) 453–467.
- [42] P.T. Eles, C.A. Michal, Two-photon two-color nuclear magnetic resonance, *J. Chem. Phys.* 121 (2004) 10167–10173.
- [43] W. Magnus, On the exponential solution of differential equations for a linear operator, *Commun. Pure Appl. Math.* 7 (1954) 649–673.
- [44] D. Possa, A.C. Gaudio, J.C.C. Freitas, Numerical simulation of NMQ/NQR spectra, 2010. <http://www.profanderson.net/files/nmr_nqr.php>.
- [45] H. Zeldes, R. Livingston, Zeeman effect on the quadrupole spectra of sodium, potassium, and barium chlorates, *J. Chem. Phys.* 26 (1957) 1102–1106.
- [46] A.D. Bain, M. Khasawneh, From NQR to NMR: the complete range of quadrupole interactions, *Concepts Magn. Reson. Part A* 22A (2004) 69–78.
- [47] T.T. Nakashima, K.J. Harris, R.E. Wasylshen, Pulse FT NMR of nonequilibrium states of half-integer spin quadrupolar nuclei in single crystals, *J. Magn. Reson.* 202 (2010) 162–172.
- [48] R. Siegel, T.T. Nakashima, R.E. Wasylshen, Sensitivity enhancement of NMR spectra of half-integer quadrupolar nuclei in the solid state via population transfer, *Concepts Magn. Reson. Part A* 26A (2005) 47–61.
- [49] R. Siegel, T.T. Nakashima, R.E. Wasylshen, Sensitivity enhancement of NMR spectra of half-integer spin quadrupolar nuclei in solids using hyperbolic secant pulses, *J. Magn. Reson.* 184 (2007) 85–100.
- [50] K.K. Dey, S. Prasad, J.T. Ash, M. Deschamps, P.J. Grandinetti, Spectral editing in solid-state MAS NMR of quadrupolar nuclei using selective satellite inversion, *J. Magn. Reson.* 185 (2007) 326–330.
- [51] N.M. Trease, K.K. Dey, P.J. Grandinetti, Optimum excitation of xxx enhanced xxx central transition populations, *J. Magn. Reson.* 200 (2009) 334–339.
- [52] S. Vega, Fictitious spin 1/2 operator formalism for multiple quantum NMR, *J. Chem. Phys.* 68 (1978) 5518–5527.
- [53] A. Wokaun, R.R. Ernst, Selective excitation and detection in multilevel spin systems: application of single transition operators, *J. Chem. Phys.* 67 (1977) 1752–1758.
- [54] M.J. Weber, E.L. Hahn, Selective spin excitation and relaxation in nuclear quadrupole resonance, *Phys. Rev.* 120 (1960) 365–375.
- [55] C.E. Hayes, The development of the birdcage resonator: a historical perspective, *NMR Biomed* 22 (2009) 908–918.
- [56] E. Knill, I.L. Chuang, R. Laflamme, Effective pure states for bulk quantum computation, *Phys. Rev. A* 57 (1998) 3348–3363.
- [57] L.M.K. Vandersypen, M.C.S. Yannoni, H.S. Sherwood, I.L. Chuang, Realization of effective pure states for bulk quantum computation, *Phys. Rev. Lett.* 83 (1999) 3085–3088.